

# Plasmon-enhanced near-field chirality in twisted van der Waals heterostructures

T. Stauber,<sup>\*,†</sup> T. Low,<sup>P</sup> and G. Gómez-Santos<sup>S</sup>

<sup>†</sup>*Departamento de Teoría y Simulación de Materiales, Instituto de Ciencia de Materiales de Madrid, CSIC, 28049 Madrid, Spain*

<sup>‡</sup>*Institute for Theoretical Physics, University of Regensburg, D-93040 Regensburg, Germany*

<sup>P</sup>*Department of Electrical & Computer Engineering, University of Minnesota, Minneapolis, Minnesota 55455, USA*

<sup>S</sup>*Departamento de Física de la Materia Condensada, INC and IFIMAC, Universidad Autónoma de Madrid, E-28049 Madrid, Spain*

E-mail: tobias.stauber@csic.es

## Abstract

It is shown that chiral plasmons, characterized by a longitudinal magnetic moment accompanying the longitudinal charge plasmon, lead to electromagnetic near-fields that are also chiral. For twisted bilayer graphene, we estimate that the near field chirality of screened plasmons can be several orders of magnitude larger than that of the related circularly polarized light. The chirality also manifests itself in a deflection angle that is formed between the direction of the plasmon propagation and its Poynting vector. Twisted van der Waals heterostructures might thus provide a novel platform to promote enantiomer-selective physio-chemical processes in chiral molecules without the application of a magnetic field or external nano-patterning that break time-reversal, mirror plane or inversion symmetry, respectively.

# Keywords

twisted bilayer graphene, plasmons, chirality, light-matter interaction

## Introduction

Chirality is an important aspect in life as only one enantiomer of amino acids is present in nature.<sup>1</sup> Furthermore, chiral objects can only be distinguished through the interaction with other chiral objects. A prominent example is the circular dichroism of chiral molecules where a different absorption cross section is seen when changing the chirality of the incident light.<sup>2-6</sup> This gives rise to an asymmetry factor denoting the normalised difference between the two absorption cross sections.

Exposing (chiral) organic molecules to circularly polarized light (CPL) might lead to modified chemical reactions, but in general the asymmetry factor is of the order of  $10^{-3}$  and thus negligible. This is related to the fact that the length scales between the two interacting chiral objects usually differ by several orders of magnitudes, i.e., for CPL  $ak \approx 10^{-3}$  in the optical regime where  $k = 2\pi/\lambda$  denotes the wave number and  $a$  the length scale of the molecule.

There have been proposals to enhance the enantioselectivity in the excitation of chiral molecules by superchiral light.<sup>7</sup> Also chiral metamaterials and plasmonics show promising results,<sup>5,8,9</sup> and even in Bernal-stacked bilayer graphene axial coupling can be induced.<sup>10</sup> But with the advent of atomically thin two-dimensional (2D) crystals,<sup>11</sup> new opportunities arise and macroscopically large chiral objects with inherent uniaxial coupling can be designed following a bottom-up approach by placing the 2D crystals on top of each other with a rotational mismatch.

The circular dichroism of twisted bilayer graphene (TBG) was first observed by Kim et al.,<sup>12</sup> but is rather weak. It could be increased by stacking multiple layers with a definite relative twist angle on top of each other. For  $n$  layers, the intrinsic length scale

given by the interlayer separation  $a \sim 3.4\text{\AA}$  would be increased by  $a \rightarrow a^* = na$  and the dimensionless chirality scale  $a^*k$  could reach the order of unity.<sup>12</sup> Another way to increase the dimensionless chirality scale  $ak$  would be to decrease the wavelength of the chiral field.

Reducing the wavelength of the electromagnetic field is possible using confined plasmonic modes. Adsorbed molecules naturally facilitates the coupling of far-field light into these plasmonic modes, and their excitation significantly enhances otherwise weak light-matter interactions.<sup>13</sup> In fact, the plasmonic wave-length can be considerably decreased in graphene,<sup>14,15</sup> which is related to the fact that the Fermi velocity  $v_F$  is two orders of magnitude smaller the speed of light  $c$ .<sup>16,17</sup> We shall be guided by this approach and introduce a new degree of freedom in the form of the chirality of the near-field by considering plasmons in twisted van der Waals heterostructures.

## Chiral plasmons in TBG

Twisted bilayer graphene<sup>18–25</sup> (TBG) has attracted tremendous attention since the discovery of correlated insulator states<sup>26,27</sup> as well as superconductivity<sup>28–30</sup> close to the magic angle of  $\theta \sim 1.08^\circ$ . Also, plasmonics in TBG has received considerable interest,<sup>17,31–33</sup> and interband collective modes around the charge neutrality point have been predicted<sup>34</sup> and observed.<sup>35</sup> Furthermore, for systems with narrow band widths such as TBG, plasmons are expected to be long-lived<sup>36,37</sup> and for twist angles of less than half a degree, the possibility of a photonic-crystal for these collective excitations opens up.<sup>38</sup> Scanned probe optical techniques can also be used to determine the local twist angle and domain structure.<sup>39</sup>

Like any metal layer, doped TBG hosts plasmons with dispersion given by  $\omega^2 = qD_T/(\epsilon_0(\epsilon_1 + \epsilon_2))$ . It depends on the dielectric constants of the upper ( $\epsilon_1$ ) and lower ( $\epsilon_2$ ) half-planes as well as on the total Drude weight or charge stiffness  $D_T$  as defined in the Supplemental Information (SI). For 2D systems with dispersion relation  $\epsilon_{\mathbf{k}} \sim |\mathbf{k}|^\nu$  and spin- and valley degeneracy  $g_s, g_v$ , it is proportional to the Fermi energy  $E_F$  with

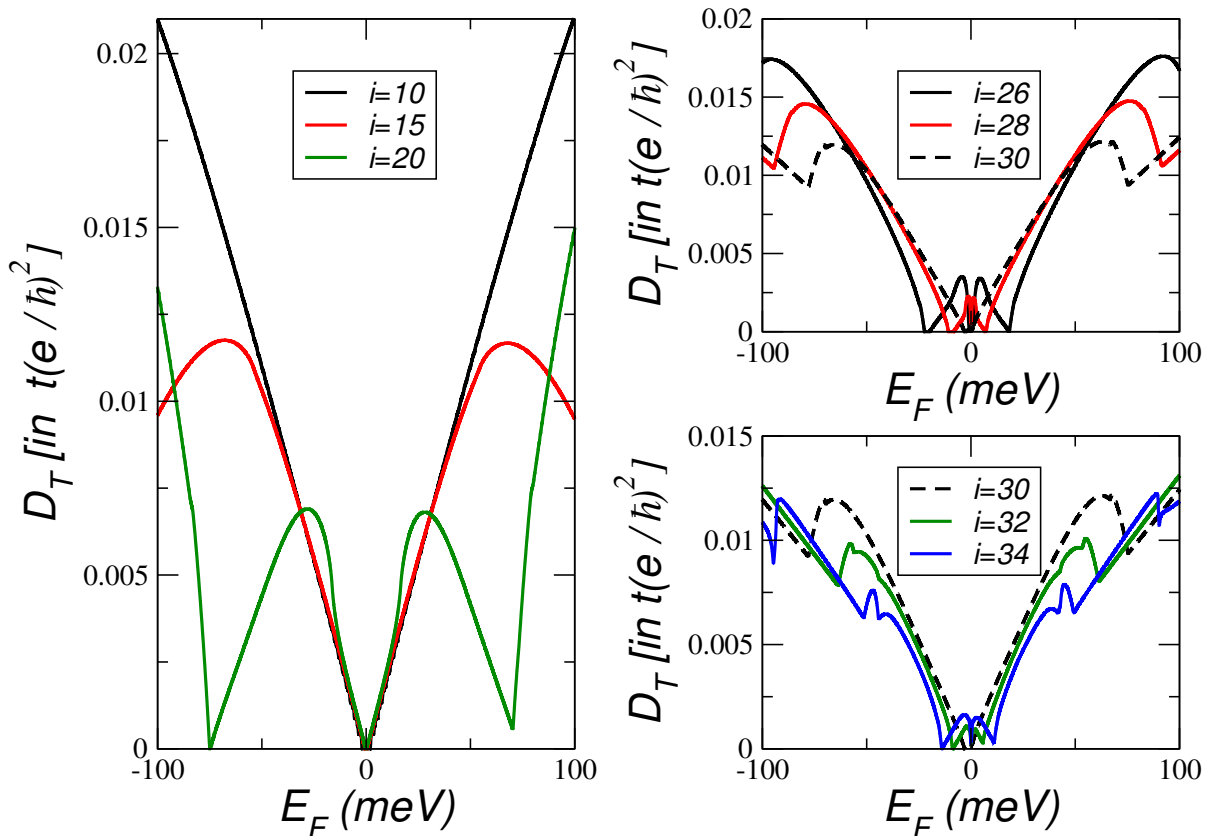


Figure 1: The total Drude weight in units of  $t(e/\hbar)^2$  for large twist angles  $\theta_i = 3.15^\circ, 2.13^\circ, 1.61^\circ$  with  $i = 10, 15, 20$  (left) and for small twist angles  $\theta_i = 1.25^\circ, 1.16^\circ, 1.08^\circ, 1.02^\circ, 0.96^\circ$  with  $i = 26, 28, 30, 32, 34$  (right) as function of the Fermi energy  $E_F$ . Commensurate twist angles are parametrised by  $\cos \theta_i = \frac{3i^2+3i+1/2}{3i^2+3i+1}$  and  $t = 2.78\text{eV}$  denotes the in-plane hopping parameter.

$D_T = \frac{g_s g_v \nu E_F}{4\pi \hbar^2}$ .<sup>17</sup> This linear behavior is strongly modified in the case of TBG due to the appearance of mini-bands<sup>31</sup> as shown in Fig. 1. Placing a metal<sup>40</sup> or a large dielectric<sup>41</sup> at a finite distance  $d$  from the TBG sheet will effectively screen the plasmons, leading to the linear dispersion relation  $\omega = v_s q$ , characterized by the sound velocity  $v_s$ .

Chiral plasmonics relies on TBG's intrinsic chirality that gives rise to circular dichroism in the absence of symmetry-breaking fields.<sup>12,42-44</sup> It is due to the small, but finite separation of the two graphene layers which requires that even the minimal response theory has to be formulated within a  $4 \times 4$  matrix as defined in the SI.<sup>33,45-47</sup> Chirality can then be discussed via the chiral Drude weight  $D_{xy}$  that links the  $x$ -direction of layer 1 to the  $y$ -direction of layer 2. This quantity is shown in Fig. 2 and can be related to the

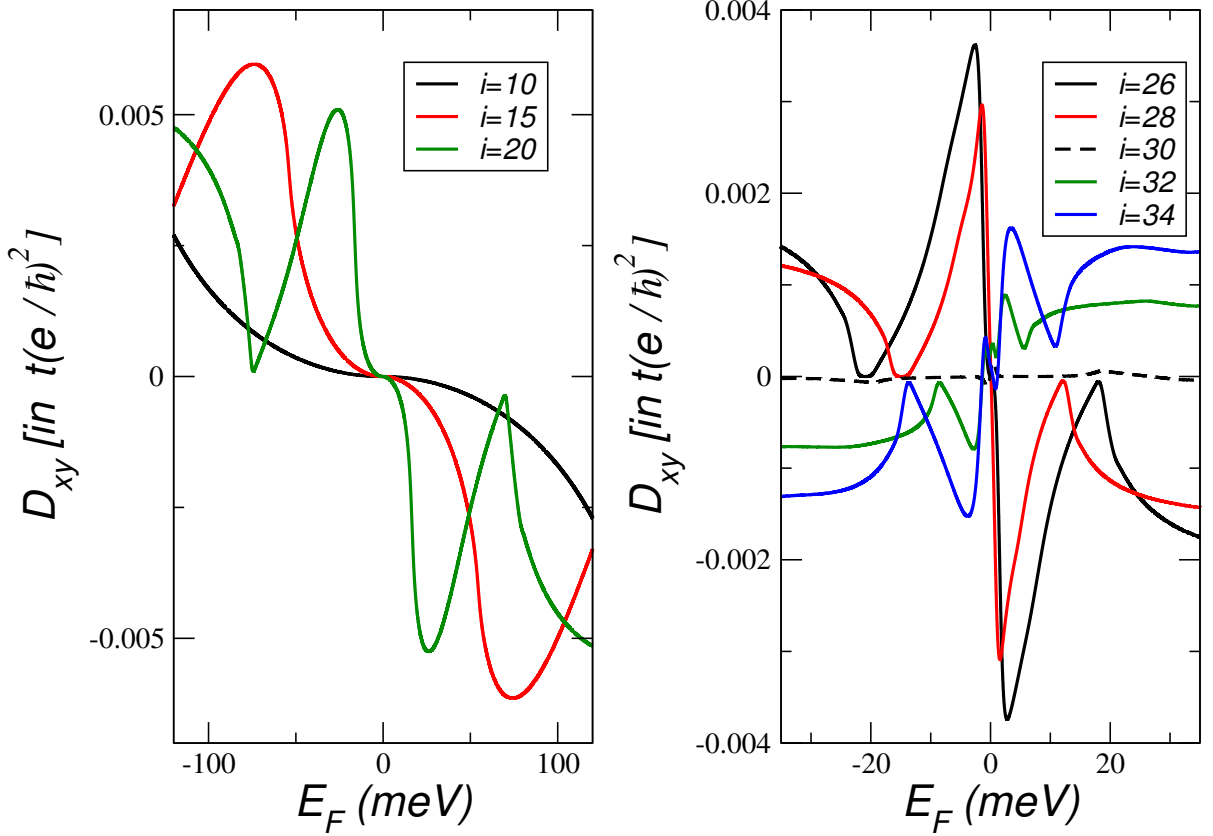


Figure 2: The chiral Drude weight in units of  $t(e/h)^2$  for large twist angles  $\theta_i = 3.15^\circ, 2.13^\circ, 1.61^\circ$  with  $i = 10, 15, 20$  (left) and for small twist angles  $\theta_i = 1.25^\circ, 1.16^\circ, 1.08^\circ, 1.02^\circ, 0.96^\circ$  with  $i = 26, 28, 30, 32, 34$  (right) as function of the Fermi energy  $E_F$ . Commensurate twist angles are parametrised by  $\cos \theta_i = \frac{3i^2+3i+1/2}{3i^2+3i+1}$  and  $t = 2.78\text{eV}$  denotes the in-plane hopping parameter.

vector-product of the sheet current densities as<sup>48</sup>

$$D_{xy} = \frac{1}{2A} \sum_{\mathbf{k}, n} \mathbf{e}_z \cdot (\mathbf{j}_{\mathbf{k}, n}^1 \times \mathbf{j}_{\mathbf{k}, n}^2) \delta(\epsilon_{\mathbf{k}, n} - E_F), \quad (1)$$

where  $\mathbf{j}_{\mathbf{k}, n}^\ell = \langle \mathbf{k}, n | \mathbf{j}^\ell | \mathbf{k}, n \rangle$  and  $\epsilon_{\mathbf{k}, n}$  and  $|\mathbf{k}, n\rangle$  denote the eigenvalues and eigenvectors, respectively, with  $\mathbf{k}$  inside the first Brillouin zone.  $A$  labels the area of the sample and  $\mathbf{j}^\ell$  is the current operator of layer  $\ell = 1, 2$ .

The chiral term  $D_{xy}$  adds a transverse component to the longitudinal current of ordinary plasmons with opposite sign in each layer, which can be viewed as a longitudinal magnetic moment.<sup>45</sup> Therefore, the chiral Drude weight of Eq. (1) endows longitudinal

plasmons of twisted structures with a chiral character by linking the electric dipole oscillations  $\mathbf{p}$  to magnetic dipole oscillations  $\mathbf{m}$  via  $\mathbf{p} \sim \mathbf{m}$ . Here, we show that this property is passed onto the electromagnetic near-field and due to the strong field confinement of graphene's surface-plasmon polaritons, the field chirality is several orders of magnitude larger than the one of the corresponding far-field. Twisted atomically thin van der Waals heterostructures may thus provide the strongest near field chirality without the need of a magnetic field<sup>49</sup> or externally breaking the mirror plane or inversion symmetry via external nano-patterning.<sup>50-52</sup>

## Near-field properties of chiral plasmons in TBG

Chiral plasmonics in twisted bilayer graphene has first been introduced and discussed in the non-retarded limit,<sup>45,46</sup> and was recently extended including relativistic effects.<sup>33</sup> The static approach is usually enough since the transverse (s-polarised) current sources are suppressed by the fine-structure constant and can thus be neglected in comparison to the longitudinal (p-polarised) current sources. However, there are quantities which are zero in the non-retarded regime and these shall be discussed in this work within the full retarded response theory.

The plasmonic field in a general bilayer is generated by the in-plane currents  $\mathbf{j}^\ell = j_\parallel^\ell \mathbf{e}_\parallel + j_\perp^\ell \mathbf{e}_\perp$  with  $\ell = 1, 2$  that carry the momentum  $\mathbf{q} = q\mathbf{e}_\parallel$  in the non-retarded limit. TBG displays chirality without breaking time-reversal symmetry and we have for the charged plasmon<sup>45,46</sup>  $j_\parallel \equiv j_\parallel^1 = j_\parallel^2$  and  $j_\perp \equiv j_\perp^1 = -j_\perp^2$ . This polarization of currents is for symmetric environments and we expect it to also roughly hold in asymmetric setups such as the one for screened plasmons discussed below.

In SI, we analyze the near-field response of one layer for which time-reversal symmetry is explicitly broken. This treatment can be extended to a bilayer with the two layers located at  $z_1 = a/2$  and  $z_2 = -a/2$  and for TBG, we set  $a = 3.4\text{\AA}$ . An alternative approach considering an effective single electro-magnetic sheet can be found in the SI.

## Local near-field chirality

The formula for the local chirality and the local chirality flux couples the longitudinal and transverse field component. For real electromagnetic fields ( $\mathcal{E}$ ,  $\mathcal{B}$ ) in a dielectric medium ( $\epsilon$ ,  $\mu$ ), it is given by<sup>53</sup>

$$\mathcal{C} = \frac{\epsilon\epsilon_0}{2} \mathcal{E} \cdot (\nabla \times \mathcal{E}) + \frac{1}{2\mu\mu_0} \mathcal{B} \cdot (\nabla \times \mathcal{B}), \quad (2)$$

$$\mathcal{F} = \frac{1}{2\mu\mu_0} (\mathcal{E} \times (\nabla \times \mathcal{B}) - \mathcal{B} \times (\nabla \times \mathcal{E})). \quad (3)$$

Both quantities are related via the continuity equation  $\partial_t \mathcal{C} + \nabla \cdot \mathcal{F} = 0$ .

We will evaluate these expressions for the near-field that is produced by the longitudinal and transverse current sources  $j_{\parallel}$  and  $j_{\perp}$ , see the SI. To be more general, we will from now on explicitly consider two different dielectrics  $\epsilon_i$ ,  $\mu_i$  with  $i = 1, 2$  in the two half-planes  $|z| > a/2$  where  $a$  denotes the distance between the two twisted atomic layers.

In the limit  $aq'_i \ll 1$  with  $q'_i = \sqrt{q^2 - (\omega/c_i)^2}$ , we then have

$$\mathcal{C}_i = -\frac{\mu_i\mu_0}{2} aq'^2 j_{\parallel} j_{\perp} e^{-2q'_i|z|}, \quad (4)$$

$$\mathcal{F}_i = -\frac{\mu_i\mu_0\omega}{2} \frac{q}{q'_i} \left[ 2j_{\parallel} j_{\perp} q'_i a \mathbf{e}_{\mathbf{q}} + sqn(z) j_{\parallel}^2 \frac{(q'_i)^2}{k_i^2} (1 + \tilde{j}_{\perp}^i) \mathbf{e}_{\mathbf{q}_{\perp}} \right] e^{-2q'_i|z|}, \quad (5)$$

where we defined  $\tilde{j}_{\perp}^i = [1 + \frac{j_{\perp}^2}{j_{\parallel}^2} \frac{k_i^2}{(q'_i)^2}] (\frac{q'_i a}{2})^2$  and  $k_i = \omega/c_i$  with  $c_i = c/\sqrt{\mu_i\epsilon_i}$  the speed of light of the dielectric medium. Related quantities such as the helicity and ellipticity can also be obtained from the above expressions, see SI. For completeness, let us also present the local energy density  $w_i$  and the local Poynting vector  $\mathbf{P}_i$  of each half-plane:

$$w_i = \frac{\mu_i\mu_0 j_{\parallel}^2}{2} \frac{q^2}{k_i^2} (1 + \tilde{j}_{\perp}^i) e^{-2q'_i|z|}, \quad (6)$$

$$\mathbf{P}_i = \frac{\mu_i\mu_0 j_{\parallel}^2}{2} \frac{q\omega}{k_i^2} \left[ (1 + \tilde{j}_{\perp}^i) \mathbf{e}_{\mathbf{q}} + sqn(z) \frac{j_{\perp}}{j_{\parallel}} q'_i a \mathbf{e}_{\mathbf{q}_{\perp}} \right] e^{-2q'_i|z|} \quad (7)$$

We note that the chirality flux as well as the Poynting vector contain a non-trivial trans-

verse component  $\mathbf{e}_{\mathbf{q}_\perp}$  which could be arbitrarily chosen without violating the respective continuity equations. The local definition of Eq. (3) and the corresponding definition of the Poynting vector thus go beyond the transport properties as was first discussed in Ref.<sup>54</sup>.

## Plasmon-induced chirality

We will now discuss the plasmon-induced chirality in twisted van der Waals structures and set for simplicity  $\mu_i = 1$ . The above equations are expressed in terms of the longitudinal and transverse current and for plasmons, they are related via  $j_\perp = -2\frac{D_{xy}}{D_T}j_\parallel$ .<sup>45,46</sup> With the knowledge of the plasmon dispersion and the linear response relation  $2i\omega j_\parallel = -D_T E$  where  $E$  denotes the in-plane electric field, the chirality can then be entirely written in terms of the field intensity and material constants.

If the twisted atomic layers are surrounded by two dielectrics, the intrinsic excitations are given by unscreened (optical) plasmons and their dispersion relation reads  $\omega^2 = qD_T/(\epsilon_0(\epsilon_1 + \epsilon_2))$ .<sup>17</sup> With  $E = E_{unscr}$ , we then obtain for the chirality

$$\mathcal{C}_i = - \left( \frac{\epsilon_1 + \epsilon_2}{2\epsilon_i} \right)^2 \frac{ak_i D_{xy}}{D_T} \epsilon_i \epsilon_0 k_i E_{unscr}^2 e^{-2q'_i |z|}. \quad (8)$$

If the twisted atomic layers are in close proximity to a metallic plate, the plasmonic excitations are screened and their dispersion is defined by the (acoustic) sound velocity via  $\omega = v_s q$ . Due to the metallic gate, the chiral near-field is only present in one half-space, say  $i = 1$ , or in between the spacer ( $i = S$ ) and with  $E = E_{scr}$ , this leads to the following chirality:

$$\mathcal{C}_i = -\alpha_{xy} \frac{D_T}{4v_s^2} E_{scr}^2 e^{-2q'_i |z|}. \quad (9)$$

where  $\alpha_{xy} = \frac{aD_{xy}}{\epsilon_0 c^2}$  may be denoted as "chiral fine-structure constant". This is a small number with  $\alpha_{xy} \sim 5 \times 10^{-4} \tilde{D}_{xy}$  and  $D_{xy} = \tilde{D}_{xy} t (e/\hbar)^2$ . Nevertheless, the large local



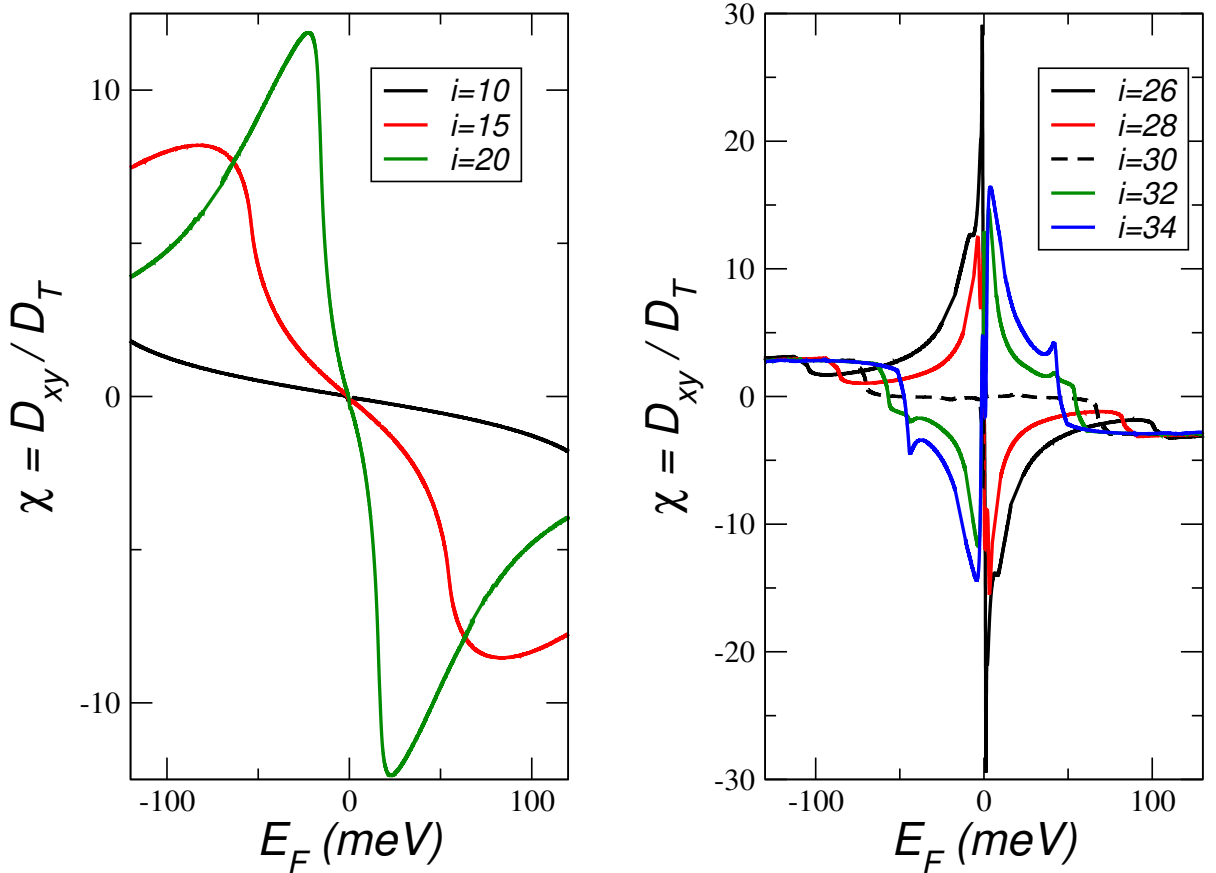


Figure 3: The dimensionless quantity  $\chi = D_{xy}/D_T$  for large twist angles  $\theta_i = 3.15^\circ, 2.13^\circ, 1.61^\circ$  with  $i = 10, 15, 20$  (left) and for small twist angles  $\theta_i = 1.25^\circ, 1.16^\circ, 1.08^\circ, 1.02^\circ, 0.96^\circ$  with  $i = 26, 28, 30, 32, 34$  (right) as function of the Fermi energy  $E_F$ . Commensurate twist angles are parametrised by  $\cos \theta_i = \frac{3i^2+3i+1/2}{3i^2+3i+1}$ .

electric field  $E_{scr}$  will lead to a strong chirality.

## Chiral deflection

The expressions for the local chirality depend on the total and chiral (Hall) Drude weight, shown in Figs. 1 and 2. In Fig. 3, we show the dimensionless chirality of the system  $\chi = D_{xy}/D_T$  that governs the relation between the longitudinal and transverse current density and thus the local chirality of (unscreened) collective charge oscillations. It also enters in the transverse component of the Poynting vector that will lead to a chiral deflection of the energy flux.

For large twist angles,  $\chi$  displays an odd behavior with a maximum of around 10. For

small twist angles, there is a constant plateau with well-defined chirality for large  $|E_F|$  reflecting the chirality of the lattice. However, around the neutrality this chirality changes sign for  $i = 30$  and  $D_{xy}$  becomes zero that was discussed in Ref.<sup>48</sup>. This opens up the possibility of detecting the magic angle by pure optical means. Notice also that the curves collapse to the same value  $|\chi| \sim 3$  for large doping independent of the twist angle.

The analytical expressions of the previous section can be simplified considerably if only the linear term in  $q'a$  is kept and retardation effects are partially neglected by  $q' \rightarrow q$ . The Poynting vector of a chiral plasmon then forms the angle  $\vartheta = -\text{sgn}(z)2\chi qa$  with respect to the propagation direction  $\mathbf{q}$ , see Eq. (7). For a twist angle of  $\theta \approx 2^\circ$  and a chemical potential around  $\mu = 40\text{meV}$ ,  $\chi \approx 10$  which would yield an angle  $\vartheta \sim 0.5^\circ$  that is formed by  $\mathbf{q}$  and  $\mathbf{P}$ . This chiral deflection should be observable via the plasmon Hall shift<sup>55</sup> at liquid-nitrogen temperatures.<sup>56</sup>

## Comparison to the chiral far-field

Let us contrast the near-field results with the chirality obtained for left (right) CPL with  $\mathbf{E}_i = E_0(1, \pm i, 0)e^{ik_i z}$  which yields  $\mathcal{C}_i^0 = \pm \epsilon_i \epsilon_0 k_i E_0^2$  and  $\mathcal{F}_i = c_i \mathcal{C}_i^0 \mathbf{e}_z$ . As might have been expected, the far-field chirality is thus proportional to the frequency  $\omega = c_i k_i$  as well as to the field intensity.

For unscreened (optical) plasmons, we have close to the interface ( $|z|q_i \ll 1$ )

$$|\mathcal{C}_i/\mathcal{C}_i^0| = \tilde{\epsilon}_i a k_i \chi F_{unscr}^2, \quad (10)$$

with the dimensionless chirality  $\chi = D_{xy}/D_T$  and relative permeability  $\tilde{\epsilon}_i = [(\epsilon_1 + \epsilon_2)/(2\epsilon_i)]^2$ . In the above formula, we have also introduced the field enhancement factor  $F_{unscr} = E_{unscr}/E_0$  for unscreened plasmons.

For screened (acoustic) plasmons, we have for the upper half-space or inside the spacer

( $i = 1, S$ )

$$|\mathcal{C}_i/\mathcal{C}_i^0| = \frac{\alpha_{xy}\alpha_T}{4\epsilon_i dk_i} F_{scr}^2, \quad (11)$$

where  $\alpha_T = \frac{dD_T}{\epsilon_0 v_s^2}$  is a constant. We have further introduced the spacer distance  $d$  for convenience and the field enhancement factor  $F_{scr} = E_{scr}/E_0$  for screened plasmons.

In the following, we will differentiate between moderately and strongly screened plasmons. In the case of moderately screened plasmons, the sound velocity is larger than the Fermi velocity  $v_s \gtrsim v_F$ . It depends on the total Drude weight and is given by  $v_s^2 = dD_T/(\epsilon_0\epsilon_S)$  which yields  $\alpha_T = \epsilon_S$ .<sup>41</sup> Note that in this case the chirality depends inversely on the spacer distance  $d$ . For strongly screened plasmons, the sound velocity approaches the Fermi velocity  $v_s \rightarrow v_F$  which sets the lower bound imposed by the non-local charge response of Dirac electrons.<sup>16,57</sup> In this case, the chirality does not depend on the distance  $d$  anymore as it has reached the physical confinement limit.

Eqs. (45) and (46) would be an artifact unless we relate both  $E = E_{unscr,scr}$  and  $E_0$  by a common physical ruler. For that, we imagine that the same plasmonic current intensity  $j_{\parallel}$  that creates  $E$ , now shines at a radiative wavevector  $q_r \ll \omega/c$ , creating the far-field plane wave of amplitude  $E_0$ . Then  $F_{scr} \sim \frac{q}{\omega/c} \sim \frac{c}{v_s}$ , valid for the typical wavevectors of graphene plasmons which will be used in the following.  $F_{scr}$  is usually larger than the one for unscreened plasmons. In an experimental setup, this can be controlled with a proximal metal plate to the TBG separated by a thin dielectric spacer. When the spacer thickness approaches 1 nm, the field confinement for the screened acoustic plasmon can be  $\sim 5$  times larger than that of the unscreened case.<sup>58</sup> In the following, we will thus set  $F_{unscr} = 0.2 \frac{c}{v_F}$ .

## Estimating near-field chirality

In Fig. 5, we plot the normalised near-field chirality with respect to the corresponding far-field chirality of circularly polarized light  $|\mathcal{C}/\mathcal{C}^0|$  for different twist angles as function

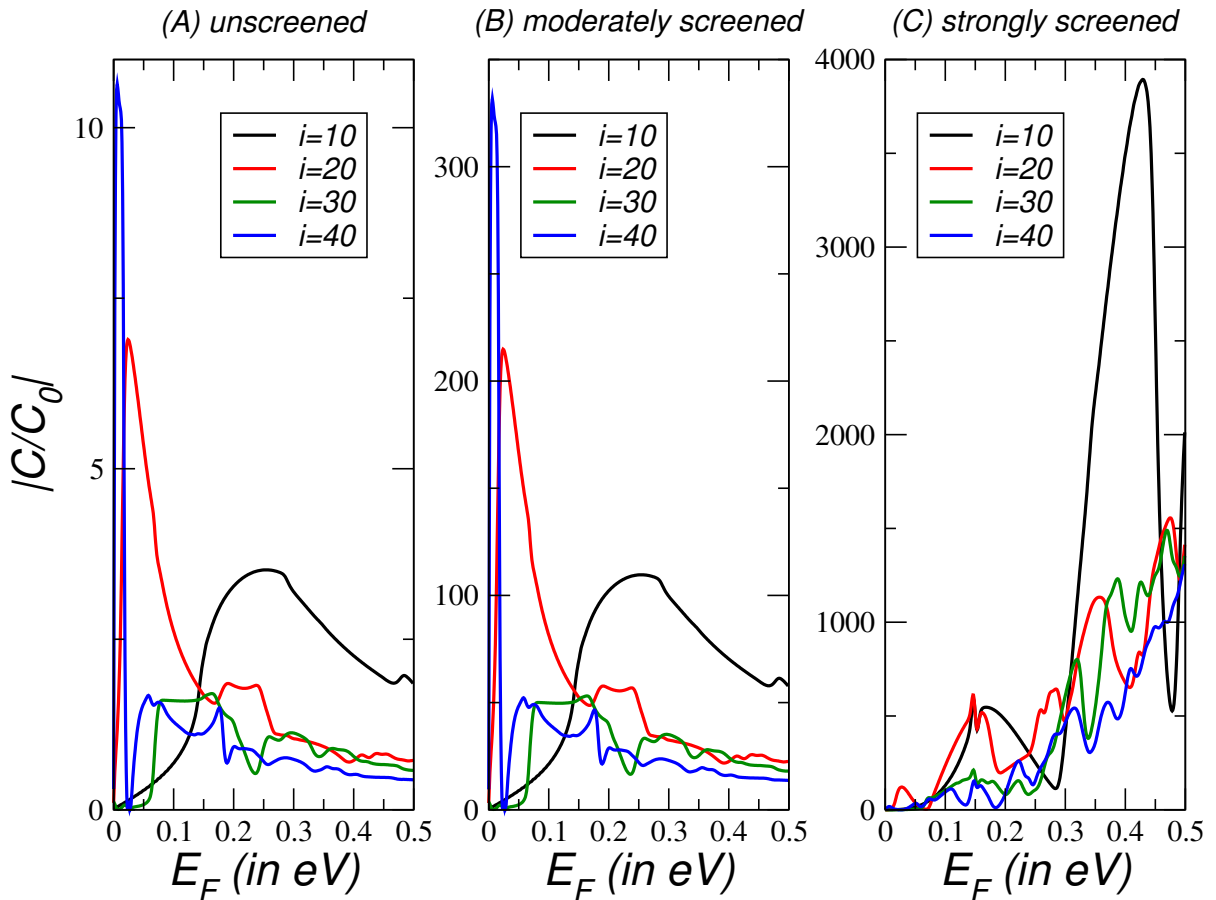


Figure 4: Near-field chirality for different plasmonic regimes normalised by the corresponding far-field chirality of circularly polarized light and different twist angles  $\theta_i = 3.15^\circ, 1.61^\circ, 1.08^\circ, 0.82^\circ$  with  $i = 10, 20, 30, 40$  as function of the Fermi energy  $E_F$ . Commensurate twist angles are parametrised by  $\cos \theta_i = \frac{3i^2+3i+1/2}{3i^2+3i+1}$ .

of the Fermi energy  $E_F$  for the half-space  $i = 1$ . This half-space is assumed to be free space with  $\epsilon_1 = 1$ . We also set  $\epsilon_2 = \epsilon_S = 5$  modelling a hBN-substrate used in typical experiments.<sup>28–30</sup> In the case of screened plasmons, we further set the spacer width to be  $\sim 5$  hBN-layers, i.e,  $d = 5a \sim 17\text{\AA}$ . Finally, we set  $\lambda_1 = 2\pi/k_1 = 10\mu\text{m}$  used in typical scanning near-field experiments,<sup>38</sup> but in the SI, also other parameters are discussed.

In Fig. 5(A), we plot the enhancement factor for unscreened plasmons which turns out to be of the order of 10. It can further be enlarged by increasing the plasmonic frequency. For moderately screened plasmons, the sound velocity  $v_s \gtrsim v_F$  is given by  $v_s^2 = dD_T/(\epsilon_0\epsilon_S)$ .<sup>41</sup> Since the field enhancement now becomes  $(c/v_s)^2 \sim D_T^{-1}$ , we obtain the same functional dependence as in the case of unscreened plasmons. However, the

enhancement factor turns out to be larger by a factor  $\sim 30$  for  $d = 5a$ , as shown in Fig. 5(B).

For strongly screened plasmons, the sound velocity approaches the Fermi velocity and we set  $v_s = v_F$ .<sup>59</sup> This yields the largest enhancement factor of the order of  $10^3$  for twist angles  $\theta \sim 3^\circ$  and for large electronic density with  $E_F \sim 0.3-0.5\text{eV}$  as shown in Fig. 5(C). Highly doped twisted van der Waals heterostructures screened by a nearby metallic gate should thus yield the strongest chiral near-field without breaking time-reversal symmetry. Moreover, the chirality is relatively broadband and highly tunable through carrier density modulation via gate voltage. Further enhancement might be possible due to the Fermi velocity renormalization by replacing  $v_F \rightarrow v_F^*$  with  $v_F^* < v_F$ .<sup>18,24</sup> Finally, let us also mention the possibility to place TBG in a cavity that should enhance the chirality at resonant frequencies.

## Chiral Chemistry

Strong light-matter interaction can induce or catalyze new reactions. E.g., there are interesting proposals to enhance two-photon processes<sup>60</sup> and to construct "designer atoms".<sup>61</sup> They rely on the wavelength reduction of confined, plasmonic excitations. An alternative, but related approach to alter chemical reactions or to catalyse new ones is to drive the system into the strong light-matter interaction regime.<sup>62-67</sup> We shall add to this general approach an additional degree of freedom, namely, the chirality of the near-field.

For screened plasmons, which can be achieved with a proximal metal gate,<sup>58,68</sup> the chiral enhancement is largest for twist angles of  $\theta \sim 3^\circ$  and for large electronic density  $n \sim 10^{13}\text{cm}^{-1}$ . This would yield an asymmetry factor in the circular dichroism of order unity and the proposed platform might give rise to unprecedented chemical reactions between chiral molecules that are usually forbidden in the spirit of previous proposals, see Fig. 5.<sup>60-67</sup>

Let us finally note that  $\mathcal{C}$  also denotes the chiral selectivity of the near-field cou-

pling with an emitter, and thus can also modify the polarized photoluminescence of dye molecules.<sup>69</sup> The adsorbed molecules which can effectively couple far-field light into the plasmons, would have different near-field coupling efficiencies for the two enantiomers.<sup>9</sup> Since the electronic chirality changes sign at the magic angle,<sup>48</sup> this selectivity can also be used to detect the magic angle by pure optical means.

## Summary and discussion

We have investigated the electromagnetic near-field confined to TBG focusing on its chirality. The rotational mismatch breaks all mirror plane symmetries and chirality arises from the quantum nature of interlayer coupling. The effect does thus not rely on the breaking of time-reversal symmetry and can, therefore, be useful in the context of catalysing chemical reactions without changing the external conditions, e.g., due to the presence of a magnetic field. We find huge field enhancements especially in the case of acoustic plasmons paving the way towards *chiral plasmon-induced chemistry* which is possible for general *twisted* van der Waals structures<sup>11</sup> since the interlayer Moiré coupling induces a chiral response that endows surface plasmons with a chiral character.<sup>33,45,46</sup> Unlike most proposals in the field of chiral plasmonics,<sup>9</sup> the near-field chirality discussed herein has a quantum origin due to the interlayer coupling between the atomic layers, and does not rely on any nanofabrication of metallic chiral structures.

Our proposal can be extended to other 2D materials beyond graphene, and provides a novel approach to macroscopic chiral platforms for optics, sensing, chemistry and beyond. One example might concern a variety of synthetic methods for amino acids that lead to equal amounts of left- and right-handed enantiomers, i.e., they are usually obtained as a racemate and processes for enantiomer separation must then be carried out if pure L- or D-amino acids are required. Performing the synthesis close to van der Waals heterostructure and exciting plasmons with a well-defined chirality might lead to enantiomerically pure L or D amino acids. Also, entirely new catalysed reaction of chiral molecules can be

envisioned.

## Acknowledgements

We thank J. González and J. Schliemann for discussions. This work has been supported by Spain's MINECO under Grant No. FIS2017-82260-P, PGC2018-096955-B-C42, and CEX2018-000805-M as well as by the CSIC Research Platform on Quantum Technologies PTI-001. TS also acknowledges support from the "Salvador de Madariaga"-Programme under Grant No. PRX19/00024 and from Germany's Deutsche Forschungsgemeinschaft (DFG) via SFB 1277. TL acknowledges support by the National Science Foundation, NSF/EFRI Grant No. EFRI-1741660.

# Supplemental Information

## Continuum model of TBG and linear response

In the following, we will perform the detailed calculations for the continuum model as proposed in Refs.<sup>18,24</sup>. For one valley, the Hamiltonian reads

$$H = \hbar v_F \begin{pmatrix} 0 & -i\partial_x - \partial_y + i\frac{\Delta\mathbf{K}}{2} & V_{AA'}(\mathbf{r}) & V_{AB'}(\mathbf{r}) \\ -i\partial_x + \partial_y - i\frac{\Delta\mathbf{K}}{2} & 0 & V_{BA'}(\mathbf{r}) & V_{AA'}(\mathbf{r}) \\ V_{AA'}^*(\mathbf{r}) & V_{BA'}^*(\mathbf{r}) & 0 & -i\partial_x - \partial_y - i\frac{\Delta\mathbf{K}}{2} \\ V_{AB'}^*(\mathbf{r}) & V_{AA'}^*(\mathbf{r}) & -i\partial_x + \partial_y + i\frac{\Delta\mathbf{K}}{2} & 0 \end{pmatrix}, \quad (12)$$

where we introduced the Fermi velocity of graphene  $v_F$ , the shift between the two Dirac cones  $\Delta\mathbf{K}$ , and  $V_{AA'}(\mathbf{r})$ ,  $V_{AB'}(\mathbf{r})$ , and  $V_{BA'}(\mathbf{r})$  are the respective interlayer tunneling amplitudes between regions of stacking  $AA$ ,  $AB$ , and  $BA$ . The Hamiltonian for the opposite valley is obtained by replacing  $\Delta\mathbf{K}$  by  $-\Delta\mathbf{K}$  and reversing the momentum  $k_x$ .

Twist angles shall be commensurate and are parametrised by  $\cos\theta_i = \frac{3i^2+3i+1/2}{3i^2+3i+1}$ . We also set the in-plane hopping parameter  $t = 2.78\text{eV}$  which is related to the Fermi velocity via  $v_F = \frac{\sqrt{3}}{2}ta_0$  with  $a_0 = 2.46\text{\AA}$ . The interlayer hopping strength is taken as  $w = 0.11\text{meV}$  following the notation of Ref.<sup>24</sup>

The conductivity  $\boldsymbol{\sigma}$  shall also be defined by a  $4 \times 4$  matrix with

$$\begin{bmatrix} \mathbf{j}^{(1)} \\ \mathbf{j}^{(2)} \end{bmatrix} = \boldsymbol{\sigma} \begin{bmatrix} \mathbf{E}^{(1)} \\ \mathbf{E}^{(2)} \end{bmatrix}, \quad (13)$$

where  $\mathbf{j}^\ell$  and  $\mathbf{E}^\ell$  represent in-plane currents and total fields in the plane  $\ell = 1, 2$ . For a rotationally invariant, symmetric system, we can then write the response in the following



way:<sup>45</sup>

$$\boldsymbol{\sigma} = \begin{pmatrix} \sigma_0 & 0 & \sigma_1 & \sigma_{xy} \\ 0 & \sigma_0 & -\sigma_{xy} & \sigma_1 \\ \sigma_1 & -\sigma_{xy} & \sigma_0 & 0 \\ \sigma_{xy} & \sigma_1 & 0 & \sigma_0 \end{pmatrix}, \quad (14)$$

where  $\sigma_{0,1}(\omega)$ ,  $\sigma_{xy}(\omega)$  are complex functions characterizing the local in-plane response. They can be interpreted as the in-plane conductivity, the covalent drag conductivity as well as the Hall or chiral conductivity, respectively.

It is usually sufficient to discuss plasmonic excitations with respect to their Drude weights and the Drude weight  $D_\nu$  is related to the low-frequency limit of the response function  $\sigma_\nu$  via  $D_\nu = \lim_{\omega \rightarrow 0} \omega \text{Im} \sigma_\nu$  with  $\nu = 0, 1, xy$ . The total Drude weight is then obtained by  $D_T = 2(D_0 + D_1)$ , and it is also given by the familiar inverse mass formula

$$D_T = \frac{1}{A} \sum_{\mathbf{k}, n} \left( \frac{e}{\hbar} \frac{\partial \epsilon_{\mathbf{k}, n}}{\partial k_x} \right)^2 \delta(\epsilon_{\mathbf{k}, n} - E_F), \quad (15)$$

which only needs the knowledge of the band-structure of the Hamiltonian Eq. (12). For the chiral response, we will use Eq. (1) of the main text.<sup>48</sup> Both quantities characterise the chiral near-field and are plotted and discussed in the main text.

## Near-field properties in 2D systems with broken time-reversal symmetry

Two-dimensional bulk plasmonic properties in systems with time-reversal symmetry cannot easily be distinguished from systems with broken time-reversal symmetry regarding their dispersion. The reason for that is that the transverse (s-polarised) current sources are suppressed by the fine-structure constant and can thus be neglected in comparison to

the longitudinal (p-polarised) current sources. Still, there are quantities which are only non-zero in the retarded regime such as the helicity, ellipticity or chirality.

Plasmons in two-dimensional systems with broken time-reversal symmetry exhibit a transverse current  $j_{\perp}$  that is associated to the longitudinal current  $j_{\parallel}$ . Let us define the complex sources  $\mathbf{j}_{\parallel} = j_{\parallel} \mathbf{e}_{\mathbf{q}} e^{i\mathbf{q}\cdot\mathbf{r}} e^{-2q'|z|}$  and  $\mathbf{j}_{\perp} = j_{\perp} \mathbf{e}_{\mathbf{q}\perp} e^{i\mathbf{q}\cdot\mathbf{r}} e^{-2q'|z|}$  with  $q' = \sqrt{q^2 - \mu\epsilon(\omega/c)^2}$  and  $\mathbf{e}_{\mathbf{q}\perp} = \mathbf{e}_z \times \mathbf{e}_{\mathbf{q}}$ . The corresponding real current densities shall be given by  $\mathbf{j}_{\nu} = \text{Re}\mathbf{j}_{\nu}$  with  $\nu = \parallel, \perp$ .

The associated near-field is given by  $\mathbf{A}_{\nu} = -\mathcal{D}_{\nu} \mathbf{j}_{\nu}$  where  $\mathcal{D}_{\nu}$  is the longitudinal ( $\nu = \parallel$ ) or transverse ( $\nu = \perp$ ) photonic propagator, respectively.<sup>41</sup> The parallel current  $j_{\parallel}$  will thus give rise to a longitudinal field and the perpendicular current  $j_{\perp}$  to a transverse field. With the total gauge field  $\mathbf{A} = \mathbf{A}_{\parallel} + \mathbf{A}_{\perp}$  and  $\mathbf{E} = i\omega\mathbf{A}$  and  $\mathbf{B} = \nabla \times \mathbf{A}$ , we thus obtain the following expression:

$$\mathbf{E} = i\omega \begin{pmatrix} -d_l j_{\parallel} \\ -d_t j_{\perp} \\ -i \text{sgn}(z) \frac{q}{q'} d_l j_{\parallel} \end{pmatrix} e^{iqx} e^{-q'|z|} \quad (16)$$

$$\mathbf{B} = \begin{pmatrix} -\text{sgn}(z) q' d_t j_{\perp} \\ -\text{sgn}(z) \frac{k_0^2}{q'} d_l j_{\parallel} \\ -iq d_t j_{\perp} \end{pmatrix} e^{iqx} e^{-q'|z|}, \quad (17)$$

where  $d_l = \frac{q'}{2\epsilon\epsilon_0\omega^2}$ ,  $d_t = -\frac{\mu\mu_0}{2q'}$ ,  $k_0 = \omega/c$  and  $\mathbf{e}_{\mathbf{q}} = \mathbf{e}_x$ .

## Optical momentum, spin, angular momentum, and helicity

The *local* energy density  $w$ , "complex" Poynting vector  $\Pi$  (the Poynting vector is defined as  $\mathbf{P}_{\text{Poy}} = \Re\Pi$ ), momentum  $\mathbf{P}$ , spin  $\mathbf{S}$ , and helicity  $\mathcal{H}$  of a monochromatic electromagnetic

wave can be defined as follows:<sup>54,70-73</sup>

$$w = \frac{\epsilon\epsilon_0}{4} \mathbf{E}^* \cdot \mathbf{E} + \frac{1}{4\mu\mu_0} \mathbf{B}^* \cdot \mathbf{B} \quad (18)$$

$$\mathbf{\Pi} = \frac{1}{2\mu\mu_0} \mathbf{E}^* \times \mathbf{B} \quad (19)$$

$$\omega \mathbf{P} = \frac{\epsilon\epsilon_0}{4} \Im \mathbf{E}^* \cdot (\nabla) \mathbf{E} + \frac{1}{4\mu\mu_0} \Im \mathbf{B}^* \cdot (\nabla) \mathbf{B} \quad (20)$$

$$\omega \mathbf{S} = \frac{\epsilon\epsilon_0}{4} \Im \mathbf{E}^* \times \mathbf{E} + \frac{1}{4\mu\mu_0} \Im \mathbf{B}^* \times \mathbf{B} \quad (21)$$

$$\omega \mathcal{H} = -\frac{1}{2\mu\mu_0} \Im \mathbf{E}^* \cdot \mathbf{B} \quad (22)$$

For the above current density, this yields the following local properties with  $\mathbf{q} = q\mathbf{e}_x$ :

$$w = \frac{\mu\mu_0 j_{\parallel}^2}{8} \frac{q^2}{k_0^2} \left( 1 + \frac{j_{\perp}^2}{j_{\parallel}^2} \frac{k_0^2}{(q')^2} \right) e^{-2q'|z|} \quad (23)$$

$$\mathbf{\Pi} = \frac{\mu\mu_0 j_{\parallel}^2}{8} \frac{q\omega}{k_0^2} \begin{pmatrix} 1 + \frac{j_{\perp}^2}{j_{\parallel}^2} \frac{k_0^2}{(q')^2} \\ \text{sgn}(z) 2 \frac{j_{\perp}}{j_{\parallel}} \\ -\text{sgn}(z) i \frac{q'}{q} \left( 1 - \frac{j_{\perp}^2}{j_{\parallel}^2} \frac{k_0^2}{(q')^2} \right) \end{pmatrix} e^{-2q'|z|} \quad (24)$$

$$\mathbf{P} = \frac{q}{\omega} w \mathbf{e}_q e^{-2q'|z|} \quad (25)$$

$$\mathbf{S} = -\text{sgn}(z) \frac{\mu\mu_0 j_{\parallel}^2}{8} \frac{1}{\omega} \frac{q}{q'} \begin{pmatrix} 2 \frac{j_{\perp}}{j_{\parallel}} \\ \frac{(q')^2}{k_0^2} \left( 1 + \frac{j_{\perp}^2}{j_{\parallel}^2} \frac{k_0^2}{(q')^2} \right) \\ 0 \end{pmatrix} e^{-2q'|z|} \quad (26)$$

$$\mathcal{H} = -\text{sgn}(z) \frac{\mu\mu_0 j_{\parallel} j_{\perp}}{4} \frac{q^2}{q' k_0^2} e^{-2q'|z|} \quad (27)$$

## Ellipticity

We can also define the ellipticity of the electric and magnetic field as follows

$$\mathcal{E}_{\mathbf{E}} = \Im \frac{\mathbf{E}^* \times \mathbf{E}}{\mathbf{E}^* \cdot \mathbf{E}} \cdot \mathbf{P}_{\text{Poy}}, \quad (28)$$

$$\mathcal{E}_{\mathbf{B}} = \Im \frac{\mathbf{B}^* \times \mathbf{B}}{\mathbf{B}^* \cdot \mathbf{B}} \cdot \mathbf{P}_{\text{Poy}}, \quad (29)$$

$$\mathcal{E} = \Im \frac{\epsilon\epsilon_0 \mathbf{E}^* \times \mathbf{E} + \frac{1}{\mu\mu_0} \mathbf{B}^* \times \mathbf{B}}{\epsilon\epsilon_0 \mathbf{E}^* \cdot \mathbf{E} + \frac{1}{\mu\mu_0} \mathbf{B}^* \cdot \mathbf{B}} \cdot \mathbf{P}_{\text{Poy}}, \quad (30)$$

with  $\mathbf{P}_{\text{Poy}} = \Re \Pi$ . Interestingly, we find  $\mathcal{E}_{\mathbf{E}} = \mathcal{E}_{\mathbf{B}}$  with

$$\mathcal{E}_{\mathbf{E}} = -\text{sgn}(z) \frac{\mu\mu_0 j_{\parallel} j_{\perp}}{4} \frac{\omega}{k_0^2} \frac{q^2}{q'}. \quad (31)$$

Even though the electric and magnetic fields are coupled, we can assign the same ellipticity to each sector. Consequently, we also have  $\mathcal{E} = \mathcal{E}_{\mathbf{E}}$ . Furthermore, there is a relation between the ellipticity and helicity with  $\mathcal{E} = \omega \mathcal{H}$ .

## Chirality

The local chirality for a real electromagnetic field in a dielectric medium ( $\epsilon, \mu$ ) is defined by<sup>53</sup>

$$\mathcal{C} = \frac{\epsilon\epsilon_0}{2} \boldsymbol{\mathcal{E}} \cdot (\nabla \times \boldsymbol{\mathcal{E}}) + \frac{1}{2\mu\mu_0} \boldsymbol{\mathcal{B}} \cdot (\nabla \times \boldsymbol{\mathcal{B}}). \quad (32)$$

Note that a finite contribution to the chirality only comes from the scalar product involving both, the longitudinal and the transverse field component which justifies the denomination of this conserved quantity. The resulting fields, therefore, display the following chirality:

$$\mathcal{C} = -\text{sgn}(z) \frac{\mu\mu_0}{4} \frac{j_{\parallel} j_{\perp} q^2}{q'} e^{-2q'|z|} \quad (33)$$

The optical chirality is associated to a flux of chirality related by the usual continuity

equation  $\partial_t \mathcal{C} + \nabla \cdot \mathcal{F} = 0$  (in the absence of material currents) which is locally defined as

$$\mathcal{F} = \frac{1}{2\mu\mu_0} (\mathcal{E} \times (\nabla \times \mathcal{B}) - \mathcal{B} \times (\nabla \times \mathcal{E})) . \quad (34)$$

For the chiral plasmon, this gives

$$\mathcal{F} = -\text{sgn}(z) \frac{\mu\mu_0\omega}{8} \frac{q}{q'} e^{-2q'|z|} \left[ 2j_{\parallel} j_{\perp} \mathbf{e}_{\mathbf{q}} + j_{\parallel}^2 \frac{(q')^2}{k_0^2} \left( 1 + \frac{j_{\perp}^2}{j_{\parallel}^2} \frac{k_0^2}{(q')^2} \right) \mathbf{e}_{\mathbf{q}_{\perp}} \right] . \quad (35)$$

Notice that we have  $\mathcal{F} = \omega^2 \mathcal{S}$  which gives rise to a conserved "spin-density"  $\mathcal{S} = \mathcal{C}/\omega^2$ .

We also have  $\mathcal{H} = \mathcal{C}/k_0^2$ . Both relations are general and obtained by noting that

$$\mathcal{C} = \frac{\epsilon\epsilon_0}{2} (\mathcal{B} \cdot \partial_t \mathcal{E} - \mathcal{E} \cdot \partial_t \mathcal{B}) = k_0^2 \mathcal{H} , \quad (36)$$

$$\mathcal{F} = \frac{\epsilon\epsilon_0}{2} \mathcal{E} \times \partial_t \mathcal{E} + \frac{1}{2\mu\mu_0} \mathcal{B} \times \partial_t \mathcal{B} = \omega^2 \mathcal{S} . \quad (37)$$

The chirality is also linked to the ellipticity with  $\mathcal{E} = \omega \mathcal{C}/k_0^2$ .

## Near-field properties in 2D systems with time-reversal symmetry

In the previous Section, we have analyzed the near-field response in one layer for which time-reversal symmetry is explicitly broken. This treatment can be extended to a bilayer system with the two layers located at  $z_1 = a/2$  and  $z_2 = -a/2$  and with opposing current densities. The whole system thus does not break time-reversal symmetry as indicated by the symmetric response matrix Eq. (14). An alternative approach considering an effective single electro-magnetic sheet can also be found in the last Section.

Let us now also explicitly consider two different dielectrics  $\epsilon_i, \mu_i$  with  $i = 1, 2$  in the two half-planes  $|z| > a/2$ . The electromagnetic field is usually characterized by the local energy density  $w_i$  and the local Poynting vector  $\mathbf{P}_i$  of each half-plane. In the limit  $aq'_i \ll 1$

with  $q'_i = \sqrt{q^2 - \mu_i \epsilon_i (\omega/c)^2}$ , we obtain the following expressions:

$$w_i = \frac{\mu_i \mu_0 j_{\parallel}^2 q^2}{2 k_i^2} (1 + \tilde{j}_{\perp}^i) e^{-2q'_i |z|}, \quad (38)$$

$$\mathbf{P}_i = \frac{\mu_i \mu_0 j_{\parallel}^2 q \omega}{2 k_i^2} \left[ (1 + \tilde{j}_{\perp}^i) \mathbf{e}_{\mathbf{q}} + s q n(z) \frac{j_{\perp}}{j_{\parallel}} q'_i a \mathbf{e}_{\mathbf{q}_{\perp}} \right] e^{-2q'_i |z|}, \quad (39)$$

where we defined  $\tilde{j}_{\perp}^i = [1 + \frac{j_{\perp}^2 k_i^2}{j_{\parallel}^2 (q'_i)^2}] (\frac{q'_i a}{2})^2$  and  $k_i = \omega/c_i$  with  $c_i = c/\sqrt{\mu_i \epsilon_i}$  the speed of light of the dielectric medium.

For the near-field chirality of TBG, we have as stated in the main text

$$\mathcal{C}_i = -\frac{\mu_i \mu_0}{2} a q^2 j_{\parallel} j_{\perp} e^{-2q'_i |z|}, \quad (40)$$

$$\mathcal{F}_i = -\frac{\mu_i \mu_0 \omega}{2} \frac{q}{q'_i} \left[ 2 j_{\parallel} j_{\perp} q'_i a \mathbf{e}_{\mathbf{q}} + s q n(z) j_{\parallel}^2 \frac{(q'_i)^2}{k_i^2} (1 + \tilde{j}_{\perp}^i) \mathbf{e}_{\mathbf{q}_{\perp}} \right] e^{-2q'_i |z|}. \quad (41)$$

Notice that the Poynting vector as well as the chirality flux contain a non-trivial transverse component which could be chosen arbitrarily without violating the continuity equation. The local definition of  $\mathbf{P}$  and  $\mathcal{F}$  thus goes beyond the transport properties.<sup>54</sup>

## Comparison to far-field chirality: Figure of merit

We will now discuss the plasmon-induced chirality in twisted van der Waals structures and as in the main text, we set  $\mu_i = 1$  for simplicity. The above equations are expressed in terms of the longitudinal and transverse current and for plasmons, they are related via  $j_{\perp} = -2 \frac{D_{xy}}{D_T} j_{\parallel}$ .<sup>45,46</sup> With the knowledge of the plasmon dispersion and the linear response relation  $2i\omega j_{\parallel} = -D_T E$  where  $E$  denotes the in-plane electric field, the chirality can then be entirely written in terms of the field intensity:

$$\mathcal{C}_i = -\frac{a \mu_0}{4} \frac{q^2}{\omega^2} D_{xy} D_T E^2 e^{-2q'_i |z|} \quad (42)$$

This expression depends on the ratio of  $q/\omega$  and thus on the nature of the plasmonic

excitation. Assuming an upper and lower dielectric with  $\epsilon_1$  and  $\epsilon_2$ , respectively, leads to the 2D dispersion relation for optical (unscreened) plasmons,  $\omega^2 = qD_T/(\epsilon_0(\epsilon_1 + \epsilon_2))$ . With  $c_i^{-2} = \epsilon_i\epsilon_0\mu_0$  and  $\omega = c_ik_i$ , this then yields

$$\mathcal{C}_i = - \left( \frac{\epsilon_1 + \epsilon_2}{2\epsilon_i} \right)^2 \frac{ak_i D_{xy}}{D_T} \epsilon_i \epsilon_0 k_i E^2 e^{-2q'_i|z|} . \quad (43)$$

Assuming a metallic gate at the distance  $d$  from the TBG, the plasmonic excitations become screened and obey a linear dispersion relation  $\omega = v_s q$ , characterized by the sound velocity  $v_s$ . The electric field is reduced by a factor  $(1 - e^{-2q'_s d})$  due to destructive interference, but at the same time strongly enhanced due to the field confinement. We will account for both effects by an effective field intensity. This yields

$$\mathcal{C}_i = - \frac{a}{4\epsilon_0} \frac{D_{xy} D_T}{c^2 v_s^2} E^2 e^{-2q'_i|z|} . \quad (44)$$

Let us now introduce a dimensionless figure of merit by comparing the near-field chirality with the corresponding far-field chirality given by  $\mathcal{C}_i^0 = \pm \epsilon_i \epsilon_0 k_i E_0^2$ . For unscreened plasmons, we then obtain

$$|\mathcal{C}_i/\mathcal{C}_i^0| = \left( \frac{\epsilon_1 + \epsilon_2}{2\epsilon_i} \right)^2 ak_i \frac{D_{xy}}{D_T} \left( \frac{E}{E_0} \right)^2 , \quad (45)$$

that reproduces Eq. (10) of the main text.

For screened (acoustic) plasmons, we have for the upper half-space or inside the spacer ( $i = 1, S$ )

$$|\mathcal{C}_i/\mathcal{C}_i^0| = \frac{a D_{xy}}{\epsilon_0 c^2} \frac{d D_T}{\epsilon_0 v_s^2} \frac{1}{4\epsilon_i d k_i} \left( \frac{E}{E_0} \right)^2 . \quad (46)$$

In Fig. 5, we show the near-field chirality for different dielectric constants  $\epsilon_1 = 1, 5$  and different (free space) wavelengths  $\lambda = 1, 10\mu\text{m}$  as function of the Fermi energy  $E_F$ . Whereas a large dielectric suppresses the overall chirality, changing the wavelength has

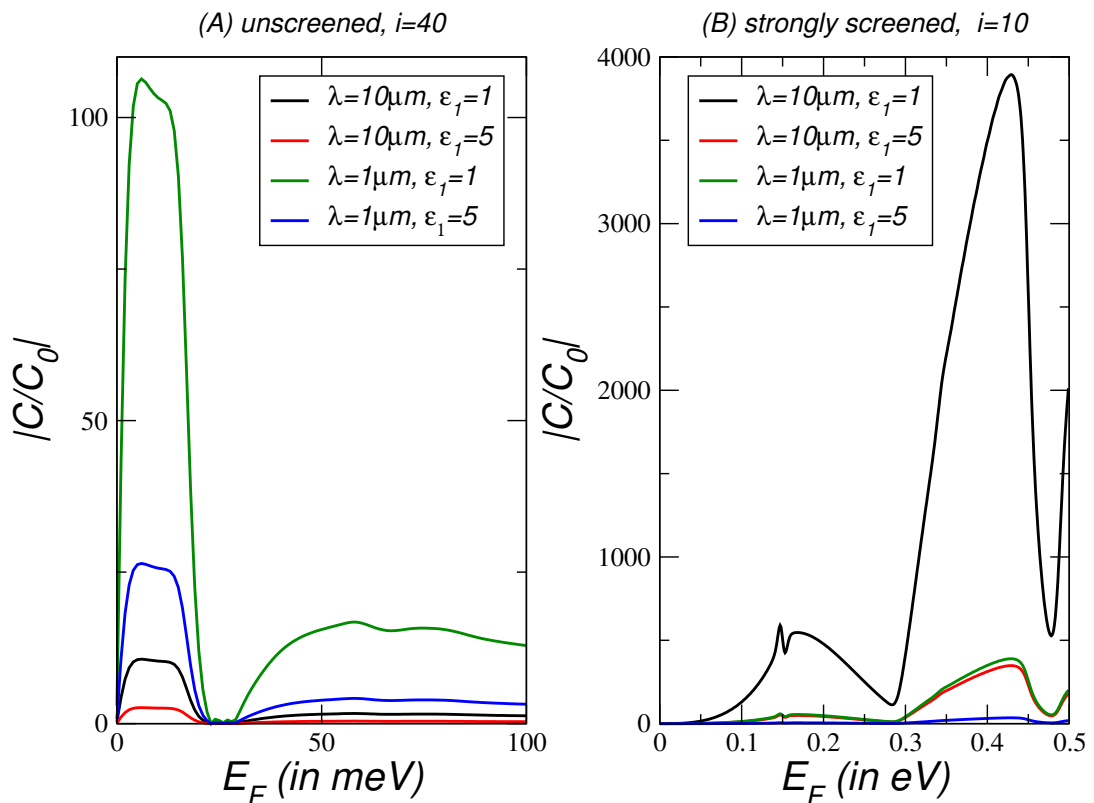


Figure 5: Near-field chirality for different plasmonic regimes normalised by the corresponding far-field chirality of circularly polarized light for different dielectric constants  $\epsilon_1 = 1, 5$  and different (free space) wavelengths  $\lambda = 1, 10\mu\text{m}$  as function of the Fermi energy  $E_F$ . (A) unscreened plasmons for  $\theta_i = 0.82^\circ$  with  $i = 40$ . (B) strongly screened plasmons for  $\theta_i = 3.15^\circ$  with  $i = 10$ .

opposite effects with respect to (A) unscreened and (B) screened plasmons.

## Chirality in magneto-electric sheets

In this Appendix, we will consider an effective magneto-electric sheet. For chiral plasmons, the classical picture of field sources in vacuum are then in-plane, longitudinal current and magnetic moment densities, written as

$$\begin{aligned}
 2\mathbf{j}(\mathbf{r}, t) &= \mathbf{j}_0 e^{i\mathbf{q}\cdot\mathbf{r}} e^{-i\omega t} + c.c. \\
 2\mathbf{m}(\mathbf{r}, t) &= a\tilde{m} \mathbf{j}_0 e^{i\mathbf{q}\cdot\mathbf{r}} e^{-i\omega t} + c.c.
 \end{aligned}
 \tag{47}$$



with  $\mathbf{j}_0 \parallel \mathbf{q}$ , and where  $\tilde{m}$  is a material constant that quantifies the parallel magnetic moment following the current.  $a$  represents an intrinsic length (interlayer distance for twisted bilayer), introduced to make  $\tilde{m}$  dimensionless.

The fields associated with these sources,  $\mathbf{E}_{\mathbf{j},\mathbf{m}}$  and  $\mathbf{B}_{\mathbf{j},\mathbf{m}}$ , can be calculated explicitly but, to show that  $\bar{\mathcal{C}}$  is non zero, and the generality of the argument, it suffices to realize that: i) only the crossed terms  $(\mathbf{j}, \mathbf{m})$  contribute to  $\bar{\mathcal{C}}$  on symmetry (parity) grounds, ii) the term from  $\mathbf{E}_{\mathbf{m}}\mathbf{B}_{\mathbf{j}}$  is smaller than the term  $\mathbf{E}_{\mathbf{j}}\mathbf{B}_{\mathbf{m}}$  by factors of  $(\frac{\omega}{qc})^2$ , iii) the electric and magnetic fields of an electric dipole can be read from the magnetic and electric counterparts of a magnetic dipole.

The last point and the relation between current and dipole density,  $\mathbf{j} = \partial_t \mathbf{p}$ , allow us to write

$$\mathbf{B}_{\mathbf{m}} = i\omega\epsilon\epsilon_0\mu\mu_0\tilde{m}a\mathbf{E}_{\mathbf{j}}, \quad (48)$$

and finally

$$\mathcal{C} = k_0^2 \frac{\epsilon\epsilon_0}{4} (\tilde{m} + \tilde{m}^*) a |\mathbf{E}_{\mathbf{j}}|^2. \quad (49)$$

We recall that  $\mathbf{E}_{\mathbf{j}}$  is the electric field associated with the longitudinal plasmon current and, for the near field, one could safely take the instantaneous approximation for it. Its explicit expression in terms of  $\mathbf{j}_0$  will lead to the standard exponential decay  $e^{-2q|z|}$  of near fields.

As a final remark, one notices that a real value of  $\tilde{m}$  is required for finite  $\bar{\mathcal{C}}$ . This implies that the magnetic moment has to have a component in phase with the plasmon longitudinal current and, therefore, the magnetic dipole density is in *quadrature* with the electric dipole density. This is precisely the condition for an atomic transition to be chirally active, so the whole picture is consistent. Furthermore, although the formalism is tailored to layered systems, the generality of the arguments implies that a chiral near field should exist whenever the sources comply with the previous requirement of parallel and in quadrature electric and magnetic moments.

## References

- (1) Barron, L. D. *Molecular Light Scattering and Optical Activity*; Cambridge University Press: Cambridge, 2004.
- (2) Kuwata-Gonokami, M.; Saito, N.; Ino, Y.; Kauranen, M.; Jefimovs, K.; Vallius, T.; Turunen, J.; Svirko, Y. Giant Optical Activity in Quasi-Two-Dimensional Planar Nanostructures. *Phys. Rev. Lett.* **2005**, *95*, 227401.
- (3) Rogacheva, A. V.; Fedotov, V. A.; Schwanecke, A. S.; Zheludev, N. I. Giant Gyrotropy due to Electromagnetic-Field Coupling in a Bilayered Chiral Structure. *Phys. Rev. Lett.* **2006**, *97*, 177401.
- (4) Govorov, A. O.; Fan, Z.; Hernandez, P.; Slocik, J. M.; Naik, R. R. Theory of Circular Dichroism of Nanomaterials Comprising Chiral Molecules and Nanocrystals: Plasmon Enhancement, Dipole Interactions, and Dielectric Effects. *Nano Lett.* **2010**, *10*, 1374–1382.
- (5) Guerrero-Martínez, A.; Auguie, B.; Alonso-Gómez, J. L.; Džolić, Z.; Gómez-Graña, S.; Žinić, M.; Cid, M. M.; Liz-Marzán, L. M. Intense Optical Activity from Three-Dimensional Chiral Ordering of Plasmonic Nanoantennas. *Angew. Chem. Int. Edit.* **2011**, *50*, 5499–5503.
- (6) Zhou, J.; Chowdhury, D. R.; Zhao, R.; Azad, A. K.; Chen, H.-T.; Soukoulis, C. M.; Taylor, A. J.; O'Hara, J. F. Terahertz chiral metamaterials with giant and dynamically tunable optical activity. *Phys. Rev. B* **2012**, *86*, 035448.
- (7) Tang, Y.; Cohen, A. E. Enhanced Enantioselectivity in Excitation of Chiral Molecules by Superchiral Light. *Science* **2011**, *332*, 333–336.
- (8) Plum, E.; Zhou, J.; Dong, J.; Fedotov, V. A.; Koschny, T.; Soukoulis, C. M.; Zheludev, N. I. Metamaterial with negative index due to chirality. *Phys. Rev. B* **2009**, *79*, 035407.

- (9) Hentschel, M.; Schäferling, M.; Duan, X.; Giessen, H.; Liu, N. Chiral plasmonics. *Science Advances* **2017**, *3*, e1602735.
- (10) Kammermeier, M.; Wenk, P.; Zülicke, U. In-plane magnetoelectric response in bilayer graphene. *Phys. Rev. B* **2019**, *100*, 075421.
- (11) Geim, A. K.; Grigorieva, I. V. Van der Waals heterostructures. *Nature* **2013**, *499*, 419 EP –.
- (12) Kim, C.-J.; A., S.-C.; Ziegler, Z.; Ogawa, Y.; Noguez, C.; Park, J. Chiral atomically thin films. *Nat. Nanotechnol.* **2016**, *11*, 520–524.
- (13) Low, T.; Avouris, P. Graphene plasmonics for terahertz to mid-infrared applications. *ACS nano* **2014**, *8*, 1086–1101.
- (14) Fei, Z.; Rodin, A. S.; Andreev, G. O.; Bao, W.; McLeod, A. S.; Wagner, M.; Zhang, L. M.; Zhao, Z.; Thiemens, M.; Dominguez, G.; Fogler, M. M.; Neto, A. H. C.; Lau, C. N.; Keilmann, F.; Basov, D. N. Gate-tuning of graphene plasmons revealed by infrared nano-imaging. *Nature* **2012**, *487*, 82–85.
- (15) Chen, J.; Badioli, M.; Alonso-Gonzalez, P.; Thongrattanasiri, S.; Huth, F.; Osmond, J.; Spasenovic, M.; Centeno, A.; Pesquera, A.; Godignon, P.; Zuru-tuza Elorza, A.; Camara, N.; de Abajo, F. J. G.; Hillenbrand, R.; Koppens, F. H. L. Optical nano-imaging of gate-tunable graphene plasmons. *Nature* **2012**, *487*, 77–81.
- (16) Wunsch, B.; Stauber, T.; Sols, F.; Guinea, F. Dynamical polarization of graphene at finite doping. *New Journal of Physics* **2006**, *8*, 318.
- (17) Stauber, T. Plasmonics in Dirac systems: from graphene to topological insulators. *Journal of Physics: Condensed Matter* **2014**, *26*, 123201.
- (18) Lopes dos Santos, J. M. B.; Peres, N. M. R.; Castro Neto, A. H. Graphene Bilayer with a Twist: Electronic Structure. *Phys. Rev. Lett.* **2007**, *99*, 256802.

- (19) Shallcross, S.; Sharma, S.; Pankratov, O. A. Quantum Interference at the Twist Boundary in Graphene. *Phys. Rev. Lett.* **2008**, *101*, 056803.
- (20) Suárez Morell, E.; Correa, J. D.; Vargas, P.; Pacheco, M.; Barticevic, Z. Flat bands in slightly twisted bilayer graphene: Tight-binding calculations. *Phys. Rev. B* **2010**, *82*, 121407.
- (21) Schmidt, H.; Lüdtke, T.; Barthold, P.; Haug, R. J. Mobilities and scattering times in decoupled graphene monolayers. *Phys. Rev. B* **2010**, *81*, 121403.
- (22) Li, G.; Luican, A.; Lopes dos Santos, J. M. B.; Castro Neto, A. H.; Reina, A.; Kong, J.; Andrei, E. Y. Observation of Van Hove singularities in twisted graphene layers. *Nat. Phys.* **2010**, *6*, 109–113.
- (23) de Laissardière, G. T.; Mayou, D.; Magaud, L. Localization of Dirac Electrons in Rotated Graphene Bilayers. *Nano Letters* **2010**, *10*, 804–808.
- (24) Bistritzer, R.; MacDonald, A. H. Moiré bands in twisted double-layer graphene. *P. Natl. Acad. Sci. Usa.* **2011**, *108*, 12233–12237.
- (25) Dean, C. R.; Wang, L.; Maher, P.; Forsythe, C.; Ghahari, F.; Gao, Y.; Katoch, J.; Ishigami, M.; Moon, P.; Koshino, M.; Taniguchi, T.; Watanabe, K.; Shepard, K. L.; Hone, J.; Kim, P. Hofstadter’s butterfly and the fractal quantum Hall effect in moiré-superlattices. *Nature* **2013**, *497*, 598 EP –.
- (26) Kim, K.; DaSilva, A.; Huang, S.; Fallahazad, B.; Larentis, S.; Taniguchi, T.; Watanabe, K.; LeRoy, B. J.; MacDonald, A. H.; Tutuc, E. Tunable moiré bands and strong correlations in small-twist-angle bilayer graphene. *Proceedings of the National Academy of Sciences* **2017**, *114*, 3364–3369.
- (27) Cao, Y.; Fatemi, V.; Demir, A.; Fang, S.; Tomarken, S. L.; Luo, J. Y.; Sanchez-Yamagishi, J. D.; Watanabe, K.; Taniguchi, T.; Kaxiras, E.; Ashoori, R. C.; Jarillo-

- Herrero, P. Correlated insulator behaviour at half-filling in magic-angle graphene superlattices. *Nature* **2018**, *556*, 80 EP –.
- (28) Cao, Y.; Fatemi, V.; Fang, S.; Watanabe, K.; Taniguchi, T.; Kaxiras, E.; Jarillo-Herrero, P. Unconventional superconductivity in magic-angle graphene superlattices. *Nature* **2018**, *556*, 43 EP –.
- (29) Yankowitz, M.; Chen, S.; Polshyn, H.; Zhang, Y.; Watanabe, K.; Taniguchi, T.; Graf, D.; Young, A. F.; Dean, C. R. Tuning superconductivity in twisted bilayer graphene. *Science* **2019**, *363*, 1059–1064.
- (30) Lu, X.; Stepanov, P.; Yang, W.; Xie, M.; Aamir, M. A.; Das, I.; Urgell, C.; Watanabe, K.; Taniguchi, T.; Zhang, G.; Bachtold, A.; MacDonald, A. H.; Efetov, D. K. Superconductors, orbital magnets and correlated states in magic-angle bilayer graphene. *Nature* **2019**, *574*, 653–657.
- (31) Stauber, T.; San-Jose, P.; Brey, L. Optical conductivity, Drude weight and plasmons in twisted graphene bilayers. *New J. Phys.* **2013**, *15*, 113050.
- (32) Hu, F.; Das, S. R.; Luan, Y.; Chung, T.-F.; Chen, Y. P.; Fei, Z. Real-Space Imaging of the Tailored Plasmons in Twisted Bilayer Graphene. *Phys. Rev. Lett.* **2017**, *119*, 247402.
- (33) Lin, X.; Liu, Z.; Stauber, T.; Gómez-Santos, G.; Gao, F.; Chen, H.; Zhang, B.; Low, T. Chiral Plasmons with Twisted Atomic Bilayers. *Phys. Rev. Lett.* **2020**, *125*, 077401.
- (34) Stauber, T.; Kohler, H. Quasi-Flat Plasmonic Bands in Twisted Bilayer Graphene. *Nano Lett.* **2016**, *16*, 6844–6849.
- (35) Hesp, N. C. H. et al. Collective excitations in twisted bilayer graphene close to the magic angle. *arXiv e-prints* **2019**, arXiv:1910.07893.

- (36) Lewandowski, C.; Levitov, L. Intrinsically undamped plasmon modes in narrow electron bands. *Proceedings of the National Academy of Sciences* **2019**, *116*, 20869–20874.
- (37) Khaliji, K.; Stauber, T.; Low, T. Plasmons and screening in finite-bandwidth two-dimensional electron gas. *Phys. Rev. B* **2020**, *102*, 125408.
- (38) Sunku, S. S.; Ni, G. X.; Jiang, B. Y.; Yoo, H.; Sternbach, A.; McLeod, A. S.; Stauber, T.; Xiong, L.; Taniguchi, T.; Watanabe, K.; Kim, P.; Fogler, M. M.; Basov, D. N. Photonic crystals for nano-light in moiré graphene superlattices. *Science* **2018**, *362*, 1153–1156.
- (39) Sunku, S. S.; McLeod, A. S.; Stauber, T.; Yoo, H.; Halbertal, D.; Ni, G.; Sternbach, A.; Jiang, B.-Y.; Taniguchi, T.; Watanabe, K.; Kim, P.; Fogler, M. M.; Basov, D. N. Nano-photocurrent Mapping of Local Electronic Structure in Twisted Bilayer Graphene. *Nano Letters* **2020**,
- (40) Principi, A.; Asgari, R.; Polini, M. Acoustic plasmons and composite hole-acoustic plasmon satellite bands in graphene on a metal gate. *Solid State Communications* **2011**, *151*, 1627 – 1630.
- (41) Stauber, T.; Gómez-Santos, G. Plasmons in layered structures including graphene. *New J. Phys.* **2012**, *14*, 105018.
- (42) Morell, E. S.; Chico, L.; Brey, L. Twisting dirac fermions: circular dichroism in bilayer graphene. *2D Materials* **2017**, *4*, 035015.
- (43) Addison, Z.; Park, J.; Mele, E. J. Twist, slip, and circular dichroism in bilayer graphene. *Phys. Rev. B* **2019**, *100*, 125418.
- (44) Ochoa, H.; Asenjo-Garcia, A. Flat bands and chiral optical response of twisted bilayer insulators. *arXiv:2002.09804* **2020**,

- (45) Stauber, T.; Low, T.; Gómez-Santos, G. Chiral Response of Twisted Bilayer Graphene. *Phys. Rev. Lett.* **2018**, *120*, 046801.
- (46) Stauber, T.; Low, T.; Gómez-Santos, G. Linear response of twisted bilayer graphene: Continuum versus tight-binding models. *Phys. Rev. B* **2018**, *98*, 195414.
- (47) Bahamon, D. A.; Gómez-Santos, G.; Stauber, T. Emergent magnetic texture in driven twisted bilayer graphene. *Nanoscale* **2020**, *12*, 15383–15392.
- (48) Stauber, T.; González, J.; Gómez-Santos, G. Change of chirality at magic angles of twisted bilayer graphene. *Phys. Rev. B* **2020**, *102*, 081404(R).
- (49) Poumirol, J. M.; Liu, P. Q.; Slipchenko, T. M.; Nikitin, A. Y.; Martin-Moreno, L.; Faist, J.; Kuzmenko, A. B. Electrically controlled terahertz magneto-optical phenomena in continuous and patterned graphene. *Nat. Commun.* **2017**, *8*, 14626.
- (50) Fan, Z.; Govorov, A. O. Plasmonic Circular Dichroism of Chiral Metal Nanoparticle Assemblies. *Nano Letters* **2010**, *10*, 2580–2587.
- (51) Kuzyk, A.; Schreiber, R.; Fan, Z.; Pardatscher, G.; Roller, E.-M.; Högele, A.; Simmel, F. C.; Govorov, A. O.; Liedl, T. DNA-based self-assembly of chiral plasmonic nanostructures with tailored optical response. *Nature* **2012**, *483*, 311–314.
- (52) Schäferling, M.; Yin, X.; Engheta, N.; Giessen, H. Helical Plasmonic Nanostructures as Prototypical Chiral Near-Field Sources. *ACS Photonics* **2014**, *1*, 530–537.
- (53) Tang, Y.; Cohen, A. E. Optical Chirality and Its Interaction with Matter. *Phys. Rev. Lett.* **2010**, *104*, 163901.
- (54) Berry, M. V. Optical currents. *Journal of Optics A: Pure and Applied Optics* **2009**, *11*, 094001.
- (55) Shi, L.-k.; Song, J. C. W. Plasmon Geometric Phase and Plasmon Hall Shift. *Phys. Rev. X* **2018**, *8*, 021020.

- (56) Ni, G. X.; McLeod, A. S.; Sun, Z.; Wang, L.; Xiong, L.; Post, K. W.; Sunku, S. S.; Jiang, B. Y.; Hone, J.; Dean, C. R.; Fogler, M. M.; Basov, D. N. Fundamental limits to graphene plasmonics. *Nature* **2018**, *557*, 530–533.
- (57) Stauber, T.; Gómez-Santos, G. Plasmons and near-field amplification in double-layer graphene. *Phys. Rev. B* **2012**, *85*, 075410.
- (58) Lee, I.-H.; Yoo, D.; Avouris, P.; Low, T.; Oh, S.-H. Graphene acoustic plasmon resonator for ultrasensitive infrared spectroscopy. *Nature nanotechnology* **2019**, *14*, 313–319.
- (59) Alcaraz Iranzo, D.; Nanot, S.; Dias, E. J. C.; Epstein, I.; Peng, C.; Efetov, D. K.; Lundeberg, M. B.; Parret, R.; Osmond, J.; Hong, J.-Y.; Kong, J.; Englund, D. R.; Peres, N. M. R.; Koppens, F. H. L. Probing the ultimate plasmon confinement limits with a van der Waals heterostructure. *Science* **2018**, *360*, 291–295.
- (60) Rivera, N.; Rosolen, G.; Joannopoulos, J. D.; Kaminer, I.; Soljačić, M. Making two-photon processes dominate one-photon processes using mid-IR phonon polaritons. *Proceedings of the National Academy of Sciences* **2017**, *114*, 13607–13612.
- (61) Chang, C.-H.; Rivera, N.; Joannopoulos, J. D.; Soljačić, M.; Kaminer, I. Constructing “Designer Atoms” via Resonant Graphene-Induced Lamb Shifts. *ACS Photonics* **2017**, *4*, 3098–3105.
- (62) Hutchison, J. A.; Schwartz, T.; Genet, C.; Devaux, E.; Ebbesen, T. W. Modifying Chemical Landscapes by Coupling to Vacuum Fields. *Angewandte Chemie International Edition* **2012**, *51*, 1592–1596.
- (63) Flick, J.; Ruggenthaler, M.; Appel, H.; Rubio, A. Atoms and molecules in cavities, from weak to strong coupling in quantum-electrodynamics (QED) chemistry. *Proceedings of the National Academy of Sciences* **2017**, *114*, 3026–3034.



- (64) Galego, J.; Garcia-Vidal, F. J.; Feist, J. Many-Molecule Reaction Triggered by a Single Photon in Polaritonic Chemistry. *Phys. Rev. Lett.* **2017**, *119*, 136001.
- (65) Flick, J.; Rivera, N.; Narang, P. Strong light-matter coupling in quantum chemistry and quantum photonics. *Nanophotonics* **2018**, *7*, 1479 – 1501.
- (66) Feist, J.; Galego, J.; Garcia-Vidal, F. J. Polaritonic Chemistry with Organic Molecules. *ACS Photonics* **2018**, *5*, 205–216.
- (67) Yuen-Zhou, J.; Menon, V. M. Polariton chemistry: Thinking inside the (photon) box. *Proceedings of the National Academy of Sciences* **2019**, *116*, 5214–5216.
- (68) Alonso-González, P. et al. Acoustic terahertz graphene plasmons revealed by photocurrent nanoscopy. *Nature Nanotechnology* **2017**, *12*, 31–35.
- (69) Meinzer, N.; Hendry, E.; Barnes, W. L. Probing the chiral nature of electromagnetic fields surrounding plasmonic nanostructures. *Physical Review B* **2013**, *88*, 041407.
- (70) Bliokh, K. Y.; Kivshar, Y. S.; Nori, F. Magnetoelectric Effects in Local Light-Matter Interactions. *Phys. Rev. Lett.* **2014**, *113*, 033601.
- (71) Bliokh, K. Y.; Bekshaev, A. Y.; Nori, F. Extraordinary momentum and spin in evanescent waves. *Nature Communications* **2014**, *5*, 3300 EP –.
- (72) Bliokh, K. Y.; Nori, F. Transverse and longitudinal angular momenta of light. *Physics Reports* **2015**, *592*, 1 – 38.
- (73) Bliokh, K. Y.; Bekshaev, A. Y.; Nori, F. Optical Momentum, Spin, and Angular Momentum in Dispersive Media. *Phys. Rev. Lett.* **2017**, *119*, 073901.